ELSEVIER

Journal of Nuclear Materials 258–263 (1998) 1856–1860

journal of nuclear materials

Mechanical properties and microstructure of α-alumina and magnesium aluminate spinel irradiated with He ions

Koichiro Izumi, Kazuhiro Yasuda *, Chiken Kinoshita, Masanori Kutsuwada

Department of Applied Quantum Physics and Nuclear Engineering, Kyushu University, Hakozaki, Fukuoka 812-8581, Japan

Abstract

Mechanical properties of α-alumina, stoichiometric- and nonstoichiometric-magnesium aluminate spinel single crystals were examined by using ultra-microhardness technique. The samples were irradiated with 100 keV He^+ ions at temperatures of 300–870 K and to fluences up to 2×10^{20} He^+/m^2. Apparent hardness, ΔH, in α-alumina increases with fluence in three stages, while that of spinel crystals increases monotonically with fluence. We have also evaluated elastic modulus, plastic and elastic energies, and plastic and elastic indentation depths through the analysis of load–displacement curves. These analyses showed that plastic and elastic hardening are responsible for the variation of ΔH of α-alumina, and that plastic hardening is the main cause of hardening in spinel crystals. Corresponding TEM observations suggested the importance of point defects and/or 'invisible' defect clusters for radiation hardening compared to 'visible' dislocation loops. The relationship between microstructure and mechanical properties is given for various ceramics.

1. Introduction

Oxide ceramics, such as α-alumina and magnesium aluminate spinel, have potential applications in fusion reactors for toroidal insulating breaks, radio frequency windows and diagnostic probes [1]. The stability of mechanical properties is, needless to say, one of the essentials to confirm the safe use of these ceramics under fusion environments. There have been, however, few systematic studies on mechanical properties of the oxide ceramics, except for limited reports on ion- and neutron-irradiated stoichiometric spinel and α-alumina [2–5].

The ultra-microhardness technique, or nanoindentation technique, is useful for measuring mechanical properties of thin surface layers and small regions of irradiated materials [6,7]. This technique also allows one to record load–displacement relation continuously during the indentation process. In the present study, we have applied the technique to study the mechanical properties of sapphire, and stoichiometric and non-stoichiometric magnesium aluminate spinel, irradiated with 100 keV He^+ ions. The load displacement curves of these ceramics are analyzed as a function of He-ion fluence and irradiation temperature, evaluating apparent hardness, elastic modulus, plastic and elastic energies dissipated during indentation process, and also the plastic and elastic indentation depths. The objectives of this study are, thus, to establish a method of analyzing the load–displacement curves in order to understand the mechanical properties of irradiated ceramics and to discuss these properties with the microstructure of the ceramics from transmission electron microscopy.

2. Experimental

Single crystals of sapphire, α-Al_2O_3 (Union Carbide), and stoichiometric and non-stoichiometric spinel, $MgO \cdot Al_2O_3$ (Union Carbide) and $MgO \cdot 2.4Al_2O_3$ (Nakazumi Crystal), were used in the present study. Flat samples with a (1 1 $\bar{2}$ 0) surface plane for sapphire and a (1 1 1) plane for spinel were prepared. They were annealed for 24 h at 1770 K for sapphire and at 1570 K for stoichiometric and nonstoichiometric spinel, following polishing to an optical finish. These samples were irradiated with 100 keV He^+ ion fluences from 2.4×10^{18} to

* Corresponding author. Tel.: +81 92 642 3773; fax: +81 92 642 3771; email: ysktne@mbox.nc.kyushu-u.ac.jp.

0022-3115/98/$19.00
PII: S0022-3115(98)00298-0

2.0×10^{20} He^+/m^2 at temperatures from 300 to 870 K. The TRIM-96 code [8] calculates the ranges of 100 keV He^+ ions in α-Al_2O_3, $MgO \cdot Al_2O_3$ and $MgO \cdot 2.4$ Al_2O_3 to be around 550 nm. The displacement threshold energy is assumed to be 25 eV for Al and Mg, and 60 eV for O for all crystals examined.

Ultra-microhardness tests were carried out at 300 K on the irradiated surfaces using an ultra-microhardness tester (ENT-1041, Elionix). For each sample, 10 indentations were made with the maximum load (P_{max}) ranging from 0.03 to 0.39 N. In these measurements, the indenter, a triangular-base diamond pyramid with a 115° included angle, was controlled by a computer to reach the preset maximum load for 10 s. The load–displacement relation was recorded continuously during the indentation process with depth- and load–measuring resolution of 1 nm and 2.45×10^{-4} N, respectively.

TEM samples were prepared by ion thinning with 4 keV Ar^+ ions. The ion-milled samples were annealed under the same condition as the hardness samples to eliminate defect clusters induced during ion-milling. The weak-beam dark-field technique was used to observe tiny defect clusters at an electron energy of 200 keV.

3. Results and discussion

Fig. 1 shows typical examples of load–displacement curves for unirradiated and He-ion irradiated α-Al_2O_3 samples at a load of 0.049 N. A large component of elastic recovery is seen in load–displacement curves both for unirradiated and irradiated samples. This large elastic recovery was seen for all samples, α-Al_2O_3, $MgO \cdot Al_2O_3$ and $MgO \cdot 2.4Al_2O_3$, and for all irradiation fluences and temperatures. As a first step of analyses, we have evaluated the apparent hardness, H, from the load–displacement curves by using the following equation:

$$H = CP_{max}/h_{max}^2, \quad (1)$$

where P_{max} is the maximum load, h_{max} the maximum indentation depth and C a geometric constant defined by the shape of the indenter. The apparent hardness defined in Eq. (1) can be, therefore, understood as a resistance for both elastic and plastic deformation.

Fig. 2 shows the difference in the apparent hardness, ΔH, between unirradiated and irradiated samples as a function of He-ion fluence at four kinds of temperatures. It is known that the plastically deformed volume extends about 5 times the indentation depth beneath the indenter [9]. The plastic indentation depth (h_p) in α-Al_2O_3 at 0.049 N, which ranges from 140 to 180 nm, corresponds to 25% to 32% of the range of 100 keV He^+ ions. The measured hardness, therefore, represents almost the averaged hardness of irradiated surface layer, though that may include some contribution from the unirradiated region. The damage distribution against the penetration depth of incident ions is not considered in the present work. In the case of room temperature irradiation in Fig. 2, three stages can be seen in the ΔH-fluence relation. ΔH increases with fluence and reaches a

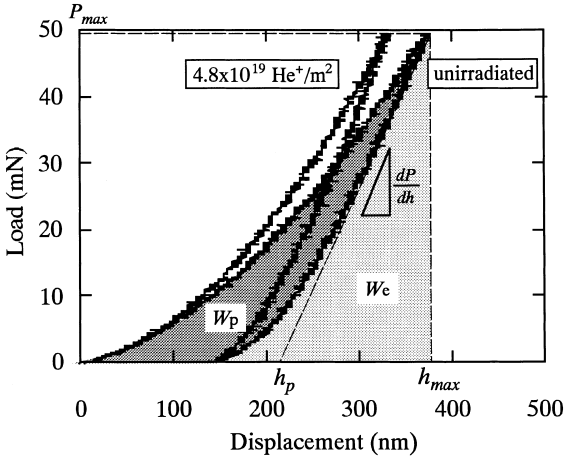

Fig. 1. Examples of load–displacement curves in α-Al_2O3 unirradiated and irradiated with 100 keV He^+ ions at 300K. The maximum load, P_{max}, is 0.049 N. Here, h_{max} is the maximum indentation depth, h_p the plastic indentation depth, h_e the elastic indentation depth ($=h_{max} - h_p$), dP/dh the slope of unloading curve, W_p the energy dissipated for plastic deformation and W_e the energy dissipated for elastic deformation.

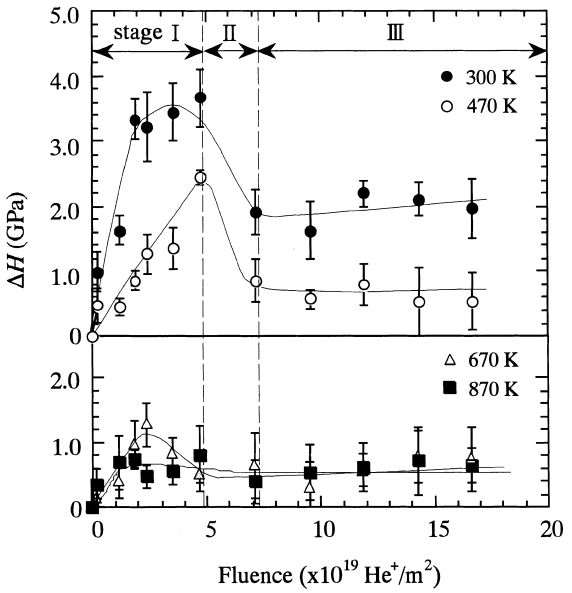

Fig. 2. Change in apparent hardness, ΔH, of α-Al_2O_3 as a function of 100 keV He-ion fluence at irradiation temperatures of 300, 470, 670 and 870 K.

maximum at 5×10^{19} He^+/m^2 (stage I). At slightly higher fluences, ΔH decreases sharply to about 60% of the maximum value (stage II). At fluences higher than 7×10^{19} He^+/m^2, ΔH increases again gradually with fluence (stage III). Similar variation of ΔH is seen against He-ion fluence at higher temperatures of 470, 670 and 870 K. However, at higher irradiation temperatures, the increment of ΔH at stage I and III decreases with increasing temperature.

Fig. 3 shows a comparison of ΔH at 300 K as a function of He-ion fluence for α-Al_2O_3, $MgO \cdot Al_2O_3$ and $MgO \cdot 2.4Al_2O_3$. In $MgO \cdot Al_2O_3$ and $MgO \cdot 2.4Al_2O_3$, the values of ΔH increase monotonically with fluence, showing a response different to that in α-Al_2O_3. In order to understand the difference in the ΔH-fluence relation between α-Al_2O_3, $MgO \cdot Al_2O_3$ and $MgO \cdot 2.4Al_2O_3$ (Figs. 2 and 3), we have tried to extract the components of plastic and elastic energies dissipated during the indentation process [10,11]. Shown in Fig. 1 as W_p and W_e are the plastic and elastic energies, respectively. W_p can be related to the energy dissipated in producing a permanent indentation by plastic deformation. W_e is, on the other hand, identified by earlier literature [12] as energy to flexure the sample surface with elastic deformation. The values of W_p and W_e are shown in Fig. 4 as a function of He-ion fluence. In Fig. 4(a), W_p in α-Al_2O_3 decreases at the beginning of irradiation and keeps a constant value up to 5×10^{19} He^+/m^2 (stage I), but then recovers to the same value as in an unirradiated sample (stage II). On the other hand, W_e in α-Al_2O_3 decreases sharply around 2×10^{19} He^+/m^2 (stage I), and gradually decreases with increasing fluence (stage II and III). Analogous variations were seen on W_p and W_e with He-ion fluence at higher temperatures of 470, 670 and 870 K. The amounts of the change in W_p and W_e, however, decreases with increasing temperature. In the cases of $MgO \cdot Al_2O_3$ and $MgO \cdot 2.4Al_2O_3$ (Fig. 4(b) and (c)), W_p decreases monotonically with increasing fluence, though W_e increases slightly with fluence in the lower fluence range and almost recovers to the level of the unirradiated sample.

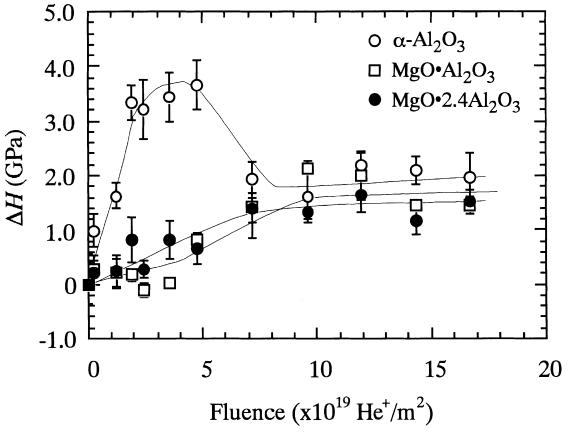

Fig. 3. Change in apparent hardness, ΔH, in α-Al_2O_3, $MgO \cdot Al_2O_3$ and $MgO \cdot 2.4Al_2O_3$ as a function of 100 keV He-ion fluence at an irradiation temperature of 300 K.

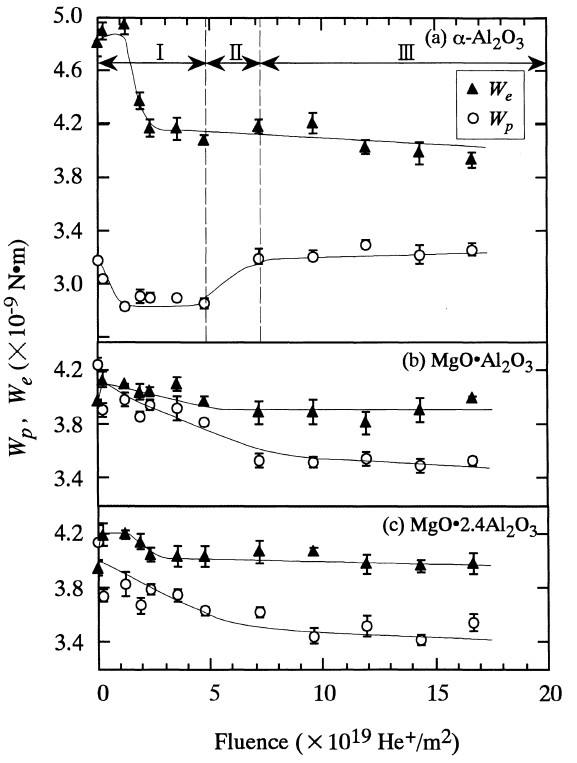

Fig. 4. Variations of W_p and W_e of (a) α-Al_2O_3, (b) $MgO \cdot Al_2O_3$ and (c) $MgO \cdot 2.4Al_2O_3$ against 100 keV He-ion fluence at an irradiation temperature of 300 K.

It can be understood, from a comparison of Figs. 2 and 4, that the increase in ΔH of α-Al_2O_3 in stage I is due to the decrease in W_p and W_e. The radiation hardening at stage I is, therefore, attributed to both plastic and elastic hardening. An analysis of unloading curves followed by the procedure reported by Page et al. [13] showed that Young's modulus increases by 30% at a fluence of 5×10^{19} He^+/m^2 (stage I) and 20% at stage III compared with the one for unirradiated sample. It is also clear that decrease in ΔH of α-Al_2O_3 at stage II is attributed to the recovery of W_p to the same level of the unirradiated sample, indicating that plastic softening is the main reason for the decrease in ΔH at stage II. Furthermore, no significant changes in W_e against fluence for $MgO \cdot Al_2O_3$ and $MgO \cdot 2.4Al_2O_3$ (Fig. 4(b) and (c)) are seen, indicating that the variation of ΔH is mainly due to the decrease of W_p with fluence.

Fig. 5 shows examples of the variation of total indentation depth (h_{max}), plastic indentation depth (h_p)

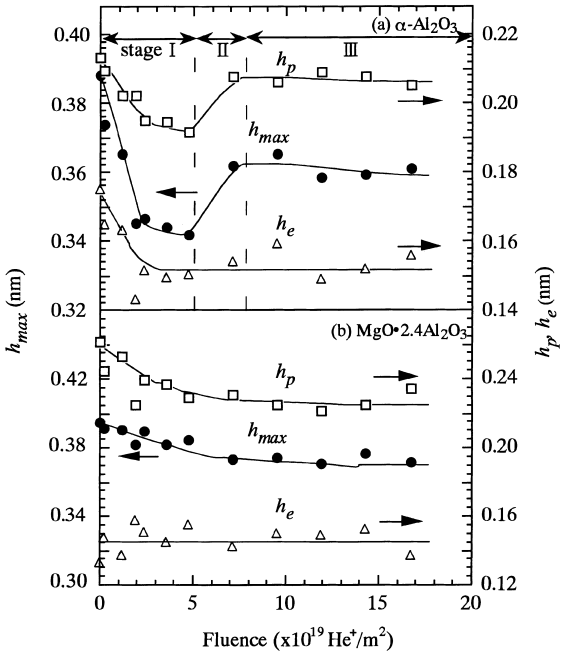

Fig. 5. Variations of h_{max}, h_p and h_e in (a) α-Al_2O_3 and (b) $MgO \cdot 2.4Al_2O_3$ against 100 keV He-ion fluence at an irradiation temperature of 300 K. The definition of h_{max} and h_p can be seen Fig. 1.

and elastic indentation depth (h_e) against He-ion fluence of α-Al_2O_3 and $MgO \cdot 2.4Al_2O_3$. Here, h_e is defined as $h_e = h_{max} - h_p$. It can be seen in Fig. 4(a) and (b) that the variation of h_p and h_e in α-Al_2O_3 and $MgO \cdot 2.4Al_2O_3$ are quite analogous to that of W_p and W_e shown in Fig. 4(a) and (c), respectively. This result indicates that the total indentation depth (h_{max}) in α-Al_2O_3 is affected by the variation of both h_p and h_e, whereas h_{max} in $MgO \cdot 2.4Al_2O_3$ is affected almost solely by h_p, confirming again that variations of ΔH (Figs. 2 and 3) are caused by plastic and elastic hardening in α-Al_2O_3 and mainly by plastic hardening in $MgO \cdot Al_2O_3$ and $MgO \cdot 2.4Al_2O_3$.

To verify our interpretation of the indentation data, TEM observations were performed. Fig. 6 shows weak-beam dark-field images of α-Al_2O_3 and $MgO \cdot Al_2O_3$ irradiated with 100 keV He^+ ions. No visible clusters are seen in α-Al_2O_3 at 300 K up to a fluence of 5×10^{19} He^+/m^2 (Fig. 6(a)). However, a high density of dot contrast images was observed at fluences higher than 7×10^{19} He^+/m^2, corresponding to stage II and III (Fig. 6(b)). The defect clusters are considered to be of interstitial type, since the mobility of vacancies is extremely low at 300 K in α-Al_2O_3 [14]. At an irradiation temperature of 870 K, a high density of black/white contrast images was observed at fluences corresponding to stage I, and their density and size increased with fluence (data are not shown). In the case of $MgO \cdot Al_2O_3$ irradiated at 300 K (Fig. 5(c)), no defect clusters were visible even at a fluence of 1×10^{20} He^+/m^2. For all samples studied, no phase transformation to an amorphous state was observed throughout the all fluences and temperatures.

These observations suggest that point defects and/or 'invisible' defect clusters by TEM are main cause for the radiation hardening of α-Al_2O_3, $MgO \cdot Al_2O_3$ and $MgO \cdot 2.4Al_2O_3$. A high density of 'visible' dislocation loops in α-Al_2O_3, on the other hand, is considered to be less effective obstacles for plastic deformation than 'invisible' defect clusters. This interpretation is consistent with the previous report by Suematsu et al. [15,16], in which they have shown point-defect induced hardening and dislocation induced softening in $MgO \cdot 3.0Al_2O_3$. It is also worthwhile noting here that the value of h_p in α-Al_2O_3 at stage III (Fig. 4(a) at irradiation temperature

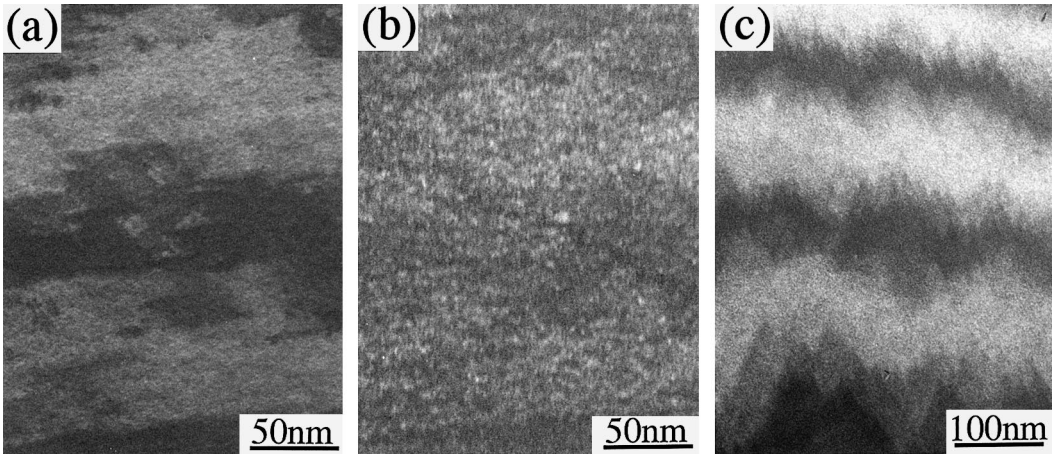

Fig. 6. Weak-beam dark-field images irradiated with 100 keV He ions: (a) α-Al_2O_3 at 300 K to a fluence of 5×10^{19} ions/m^2, (b) α-Al_2O_3 at 300 K to a fluence of 2×10^{20} ions/m^2 and (c) $MgO \cdot Al_2O_3$ at 300 K to a fluence of 1×10^{20} ions/m^2.

of 300 K) is smaller than that of the unirradiated sample, whereas W_p shows the same value with the unirradiated sample at stage III. This indicates that a smaller size indentation was made at stage III in α-Al_2O_3 than in the unirradiated sample while dissipating the same amounts of plastic energy. Dislocation loops in α-Al_2O_3 are, therefore, considered to not only enhance the generation and/or multiplication of slip dislocations in stage II but to also play a role as obstacles for work-hardening in stage III.

It has been shown by a molecular dynamic simulation study in ionic crystals [17] that both interstitials and vacancies are responsible to volumetric expansion due to the long range Coulomb interaction. The point defects in ionic crystals can, therefore, be attributed to both plastic and elastic hardening. However, the number of interstitials retained in the form of dislocation loops is found to be only 0.002–0.09% in neutron-irradiated $MgO \cdot Al_2O_3$ [18]. The exceptional high recombination rate of point defects in spinel crystals explains no significant changes in microstructure of $MgO \cdot Al_2O_3$ at 300 K (Fig. 6(c)), and this is probably the reason why spinel crystals do not show the remarkable hardening observed in α-Al_2O_3 at lower fluences. The low concentration of point defects in spinel crystals at lower fluences can also be responsible to the stability of elastic properties, as reported in neutron-irradiated $MgO \cdot Al_2O_3$ [4], leading to the difference in the radiation hardening mechanism among α-Al_2O_3, $MgO \cdot Al_2O_3$ and $MgO \cdot 2.4Al_2O_3$.

4. Conclusion

We have examined mechanical properties of α-Al_2O_3, $MgO \cdot Al_2O_3$ and $MgO \cdot 2.4Al_2O_3$ irradiated with 100 keV He^+ ions by using the ultra-microhardness technique. The followings are concluded in this study from the analyses of the load–displacement curves and a comparison of the mechanical properties with the microstructure evolution.

1. The apparent hardness, ΔH, of α-Al_2O_3 has three stages which evolves as a function of fluence, whereas ΔH of $MgO \cdot Al_2O_3$ and $MgO \cdot 2.4Al_2O_3$ increases monotonically with fluence.
2. Plastic and elastic hardening are responsible to the variation of ΔH of α-Al_2O_3, whereas plastic hardening is the main hardening mechanism in $MgO \cdot Al_2O_3$ and $MgO \cdot 2.4Al_2O_3$.
3. Point defects and/or 'invisible' defect clusters are more effective in radiation hardening rather than the 'visible' dislocation loops. The decrease in ΔH of α-Al_2O_3 at stage II can be explained from the decrease in point defect concentration due to the aggregation to dislocation loops. The difference in the recombination rate of point defects among α-Al_2O_3, $MgO \cdot Al_2O_3$ and $MgO \cdot 2.4Al_2O_3$ is probably the reason for the difference in the hardening mechanism.

Acknowledgements

This work was supported in part by Grant-in-Aid for Scientific Research (A) from the Ministry of Education, Science, Sports and Culture in Japan and Iketani Science and Technology Foundation.

References

[1] F.W. Clinard Jr., L.W. Hobbs, in: R.A. Johnson, A.N. Orlov (Eds.), Physics of Radiation Effects in Crystals, Elsevier, Amsterdam, 1986, p. 387.
[2] W. Dienst, J. Nucl. Mater. 211 (1994) 186.
[3] F.W. Clinard, Jr., W. Dienst, E.H. Farnum, J. Nucl. Mater. 212–215 (1994) 1075.
[4] Z. Li, S.K. Chan, F.A. Garner, R.C. Bradt, J. Nucl. Mater. 219 (1995) 139.
[5] R. Devanathan, N. Yu, K. Sickafus, M. Nastasi, J. Nucl. Mater. 232 (1996) 59.
[6] K. Yasuda, K. Shinohara, C. Kinoshita, M. Yamada, J. Nucl. Mater. 212–215 (1994) 1703.
[7] D.H. Plantz, L.M. Wang, R.A. Dodd, G.L. Kulcinski, Metall. Trans. A 20 (1989) 2681.
[8] J.F. Ziegler, J.P. Biersack, U. Littmark, The Stopping and Range of Ions Solids, Pergamon, New York, 1985.
[9] W.D. Nix, Metall. Trans. A 20 (1989) 2217.
[10] R. Berriche, Scripta Metall. 32 (1995) 617.
[11] J. Mencik, M.V. Swain, Mater. Forum 18 (1994) 277.
[12] W.C. Oliver, C.J. McHargue, G.C. Farlow, C.W. White, Mater. Res. Soc. Symp. Proc. 24 (1984) 515.
[13] T.F. Page, W.C. Oliver, C.J. McHargue, J. Mater. Res. 7 (1992) 450.
[14] S.J. Zinkle, C. Kinoshita, J. Nucl. Mater. 251 (1997) 200.
[15] H. Suematsu, T. Iseki, T. Yano, T. Saito, Y. Suzuki, T. Mori, J. Am. Ceram. Soc. 75 (1992) 1742.
[16] H. Suematsu, T. Suzuki, T. Iseki, T. Mori, J. Am. Ceram. Soc. 72 (1989) 306.
[17] C. Kinoshita, J. Nucl. Mater. 191–194 (1992) 67.
[18] C. Kinoshita, K. Fukumoto, K. Nakai, Ann. Chim. Fr. 16 (1991) 379.